Monte Carlo study of phase separation in aqueous protein solutions

Aleksey Lomakin, Neer Asherie, and George B. Benedek
Department of Physics and Center for Materials Science and Engineering, Massachusetts Institute of Technology, Cambridge, Massachusetts 02139-4307

(Received 11 July 1995; accepted 18 October 1995)

The binary liquid phase separation of aqueous solutions of γ-crystallins is utilized to gain insight into the microscopic interactions between these proteins. The interactions are modeled by a square-well potential with reduced range λ and depth ϵ. A comparison is made between the experimentally determined phase diagram and the results of a modified Monte Carlo procedure which combines simulations with analytic techniques. The simplicity and economy of the procedure make it practical to investigate the effect on the phase diagram of an essentially continuous variation of λ in the domain $1.05 \leqslant \lambda \leqslant 2.40$. The coexistence curves are calculated and are in good agreement with the information available from previous standard Monte Carlo simulations conducted at a few specific values of λ. Analysis of the experimental data for the critical volume fractions of the γ-crystallins permits the determination of the actual range of interaction appropriate for these proteins. A comparison of the experimental and calculated widths of the coexistence curves suggests a significant contribution from anisotropy in the real interaction potential of the γ-crystallins. The dependence of the critical volume fraction ϕ_c and the reduced critical energy $\hat{\epsilon}_c$ upon the reduced range λ is also analyzed in the context of two ''limiting'' cases; mean field theory ($\lambda \to \infty$) and the Baxter adhesive sphere model ($\lambda \to 1$). Mean field theory fails to describe both the value of ϕ_c and the width of the coexistence curve of the γ-crystallins. This is consistent with the observation that mean field is no longer applicable when $\lambda \leqslant 1.65$. In the opposite case, $\lambda \to 1$, the critical parameters are obtained for ranges much shorter than those investigated in the literature. This allows a reliable determination of the critical volume fraction in the adhesive sphere limit, $\phi_c(\lambda = 1) = 0.266 \pm 0.009$. [S0021-9606(96)50804-7]

I. INTRODUCTION

The liquid–liquid phase separation of protein solutions is of great interest because the factors which govern the condensation of protein into coexisting protein-poor and protein-rich phases are believed to play a central role in several human diseases.[1–3] The understanding of the location of the phase boundaries and the strategies to shift them by modifying protein interactions are key elements in the search for disease treatment. An important example of such a disease is cataract,[1] where opacification of the eye lens results from alterations in the spatial distribution of the lens proteins.[4] These alterations are known to be produced, in part, by the phase separation of the γ-crystallins, a family of monomeric lens proteins.[5] Several studies[6–9] have investigated the phase separation in aqueous solutions of individual members of the calf lens γ-crystallin family. These experiments show that the γ-crystallins may be divided into two groups, ''high-T_c'' proteins, such as γ_{IIIa} (γ_{C}) and γ_{IVa} (γ_{E}), which exhibit high critical temperatures ($T_c \approx 38\,^{\circ}C$), and ''low-$T_c$'' proteins, such as γ_{II} (γ_{B}) and γ_{IIIb} (γ_{D}), which exhibit low critical temperatures ($T_c \approx 5\,^{\circ}C$). The critical volume fractions of all the γ-crystallins are approximately the same $\phi_c = 0.21 \pm 0.02$.[7] The coexistence curves are found to be upper consolute and very broad, as is observed in some colloidal dispersions.[10,11] Mixtures of γ-crystallins have also been studied.[12]

From a theoretical point of view, the phase transition in the protein–water solution is analogous to that of the single component liquid–vapor system. Beginning with the van der Waals equation of state,[13] there has been a quest for an analytical equation of state for simple liquids. The general approach is to assume a form for the intermolecular potential, almost always central and pairwise additive. One of the most common selections is the square-well potential, since it is the simplest model which includes both attractive and repulsive forces. At this stage, either one of two choices is made; (i) A ''fundamental'' statistical-mechanical equation, such as the Percus–Yevick formula,[14] is invoked, from which a closed form solution for the equation of state is obtained;[15,16] (ii) A statistical-mechanical perturbation theory is used. Here, the main approach is to treat the attractive part of the potential being studied as a perturbation to the hard sphere model, which has only repulsive forces.[17–19]

Though these theories provide a recipe for how to calculate quantities of interest for phase separation, their complexity limits their utility when interpreting experimental results. One way to overcome this difficulty, is to begin with a phenomenological thermodynamic expression for the Gibbs free energy of the system. A simple analytic model, based on mean field theory, has been proposed[8,20] to describe the phase separation phenomena of aqueous protein solutions. As we shall see in this paper, this model corresponds to a long-range square-well intermolecular potential.

Many Monte Carlo simulations have been made of systems which undergo phase separation.[21–23] The most recent of these[24–26] have employed the so-called Gibbs ensemble Monte Carlo technique.[27,28] The focus of many of these stud-

 0021-9606/96/104(4)/1646/11/$6.00

ies is to examine the theory of critical phenomena for a variety of intermolecular potentials, including the square-well potential. In the recent study of Vega *et al.*,[24] the vapor–liquid phase equilibria of square-well systems with hard-sphere cores were studied for the reduced ranges $\lambda=1.25$, 1.375, 1.5, 1.75, and 2. The critical points and the shapes of the coexistence curves (in terms of a critical exponent) were calculated. This information indicates that the interactions between the γ-crystallins are short-ranged as expected. The results, however, are not detailed enough in the short-range regime to interpret the phase diagram of these proteins.

Therefore, in order to gain insight into the microscopic interactions of the γ-crystallins, we have developed our Monte Carlo method to analyze the experimental observations of Broide *et al.*[7] We also explore the applicability of mean field models, such as that proposed by Berland *et al.*[8] and Taratuta *et al.*,[20] to aqueous γ-crystallin solutions. To simplify the analysis, as well as to save computational time, our Monte Carlo procedure uses theoretical extrapolation techniques, in addition to simulation, to calculate the quantities of interest, most importantly the chemical potential. To reconstruct the phase diagram of our model aqueous protein solution, we fit the Monte Carlo results for the chemical potential with an analytic expression. We then obtain the coexistence curve by a method analogous to the Maxwell equal areas construction for the van der Waals equation of state.[29] Since the use of an analytic form for the chemical potential neglects the contributions of critical fluctuations to the free energy of the system, our approach is unable to describe accurately the critical exponents. However, we are interested in aspects of phase separation which are not strongly affected by the fluctuations; the critical temperature T_c, the critical volume fraction ϕ_c, and the shape of the coexistence curve in regions relatively far from the critical point. To check the accuracy of our method, especially near the critical point, where the reliability of the method cannot be justified *a priori*, in Sec. III B we compare our results with those available from other Monte Carlo simulations.

To begin our analysis, let us consider a system containing N_p protein molecules and N_w water molecules. We may write the microscopic free energy, E, of the protein–water solution as

$$E=E_{\rm int}+N_wE_w^{0,w}+N_pE_p^{0,w}. \tag{1}$$

This form of the microscopic free energy represents a thermodynamic average of the energy of the system over all the positions of the water molecules and over the internal degrees of freedom of the proteins. Thus, E depends solely on the relative positions of the proteins. Here $E_w^{0,w}$ is the average free energy per water molecule in a solution of pure water (i.e., the chemical potential of one water molecule) and $E_p^{0,w}$ is the average free energy of one protein molecule, fixed in space, in a dilute water solution. The interaction energy $E_{\rm int}$ results from the direct and indirect (i.e., through water) interactions between the proteins. The contribution of the water–water and protein–water interactions is independent of the positions of the proteins. However, $E_{\rm int}$ depends on the positions of the proteins and we will assume that it can be represented by a central and pairwise interaction. For convenience, we will refer to the microscopic free energy E as simply the energy of the proteins.

Now we proceed to make the model more specific. We consider the proteins to be spheres, of diameter σ, while the water is taken to be a continuous background (that is, the size of the water molecules is taken to be small as compared to σ). We assume that the effective potential energy $u(r)$ for a pair of proteins whose centers are separated by a distance r, is of the form of a square-well plus a hard core as given by Eq. (2) below,

$$u(r)=\begin{cases}+\infty, & \text{for } r<\sigma\\ -\epsilon, & \text{for } \sigma\leqslant r<\lambda\sigma\\ 0, & \text{for } r\geqslant\lambda\sigma.\end{cases} \tag{2}$$

Here λ is the reduced range of the potential well and ϵ is its depth. With this potential, we can calculate the interaction energy $E_{\rm int}$, and hence the total energy E, as a function of volume fraction and temperature. Note that for our particular choice of potential, we can define the number of protein–protein contacts $N_{\rm con}$ as the number of protein pairs whose centers are in the range $\sigma\leqslant r<\lambda\sigma$ from each other. Thus we may write the interaction energy as

$$E_{\rm int}=-N_{\rm con}\epsilon. \tag{3}$$

Of course Eq. (3) assumes that there are no overlapping hard cores in the configuration. If this is not the case and there are overlaps then $E_{\rm int}=\infty$.

Once we have chosen an explicit form for the intermolecular potential of the system, we may use the Monte Carlo simulation procedure described in Sec. II to obtain the thermodynamic properties of our system. Thus we can reconstruct the phase diagram of our model aqueous protein solution and compare it with the experimental results of Broide *et al.*[7] This comparison is made in Sec. III D.

II. COMPUTER SIMULATION

The conditions for phase equilibrium in the protein–water solution are

$$\mu_p(\mathrm{I})=\mu_p(\mathrm{II}), \tag{4}$$

$$\mu_w(\mathrm{I})=\mu_w(\mathrm{II}), \tag{5}$$

where μ_p and μ_w are the chemical potentials of the protein and water, respectively. Here I and II denote the two coexisting phases. We also write as a shorthand $\mu_p(\mathrm{I})\equiv\mu_p(\phi^{\mathrm{I}},T)$ and $\mu_p(\mathrm{II})\equiv\mu_p(\phi^{\mathrm{II}},T)$ and similarly for μ_w. We let ϕ^{I} and ϕ^{II} be the protein volume fractions in the two phases and we take $\phi^{\mathrm{I}}\leqslant\phi^{\mathrm{II}}$ without loss of generality. The temperature of the system is denoted by T. We may write Eqs. (4) and (5) in an alternative form, namely

$$\mu(\mathrm{I})=\mu(\mathrm{II}), \tag{6}$$

$$\int_{\phi^{\mathrm{I}}}^{\phi^{\mathrm{II}}}\mu(\phi,T)\,d\phi=\left(\frac{\phi^{\mathrm{II}}-\phi^{\mathrm{I}}}{2}\right)[\mu(\mathrm{I})+\mu(\mathrm{II})]. \tag{7}$$

Here $\mu \equiv \mu_p - \gamma \mu_w$, where $\gamma \equiv \Omega_p / \Omega_w$, is the ratio of the volume of one protein molecule (Ω_p) to the volume of one water molecule (Ω_w). The volume fraction is defined as $\phi \equiv N_p \Omega_p / V$, with V the total volume of the system. Equation (6) follows directly from Eqs. (4) and (5). Equation (7) is equivalent to the equal areas rule proposed by Maxwell[29] for a pure fluid and can be derived by integrating by parts the Gibbs–Duhem relation, $\phi(\partial \mu / \partial \phi) + \gamma(\partial \mu_w / \partial \phi) = 0$, from ϕ^{I} to ϕ^{II} and using Eqs. (5) and (6). The quantity μ represents the change in free energy due to the replacement of γ water molecules by one protein molecule and it is the analog of the chemical potential in a one component system. We will call μ "the effective chemical potential" to distinguish it from the protein or water chemical potentials.

We can see that in order to use Eqs. (6) and (7) to study the phase separation of the system, we need to know the effective chemical potential as an analytic function of volume fraction and temperature. We should note that below the critical temperature T_c the effective chemical potential, as an analytic function of the volume fraction, has a region of negative slope. In this region, the system is unstable to microscopic fluctuations. At the critical temperature, this region reduces to a point with critical volume fraction ϕ_c. At the critical point, both the first and second derivatives of the effective chemical potential with respect to volume fraction are zero. Thus, the two equations

$$\left. \frac{\partial \mu}{\partial \phi} \right|_{\phi_c, T_c} = 0, \tag{8}$$

$$\left. \frac{\partial^2 \mu}{\partial \phi^2} \right|_{\phi_c, T_c} = 0, \tag{9}$$

determine the values of ϕ_c and T_c. The spinodal, which marks the boundary between areas of the phase diagram where the system is stable and unstable, is given by

$$\frac{\partial \mu}{\partial \phi} = 0. \tag{10}$$

According to Eqs. (6)–(10), if μ is known as a function of ϕ and T, then the whole phase diagram may be constructed. By focusing our attention on μ, we may simplify the study of the phase separation phenomena as follows:

(i) We obtain the effective chemical potential, $\mu(\phi, T_0)$, as a function of volume fraction at a temperature T_0 above T_c, by using Widom's formula,[30]

$$\mu = \mu_0 + kT \ln \phi - kT \ln \langle \exp(-\Delta E^{\mathrm{test}} / kT) \rangle. \tag{11}$$

Here, $\langle\ \rangle$ denotes a canonical ensemble average for the system at constant volume and temperature and ΔE^{test} is the change in the microscopic free energy of the system due to the addition of a test particle. The standard part of the chemical potential is given by μ_0 and it is independent of volume fraction.

For our particular system

$$\Delta E^{\mathrm{test}} \equiv E(N_p + 1, N_w - \gamma) - E(N_p, N_w). \tag{12}$$

Using Eqs. (1) and (3) we obtain

$$\Delta E^{\mathrm{test}} = -\nu \epsilon + E_p^{0,w} - \gamma E_w^{0,w}, \tag{13}$$

where ν, the number of new contacts made by the test protein, is given by

$$\nu \equiv N_{\mathrm{con}}(N_p + 1) - N_{\mathrm{con}}(N_p). \tag{14}$$

We note that Eq. (13) presupposes that the hard core of the test protein does not overlap with any other hard core. In the case of an overlap $\Delta E^{\mathrm{test}} = \infty$. Substituting Eq. (13) into Eq. (11), we obtain the following form for the chemical potential

$$\mu = \mu_0 + E_p^{0,w} - \gamma E_w^{0,w} + kT[\ln \phi - \ln \langle \exp(\nu \hat{\epsilon}) \rangle], \tag{15}$$

where $\hat{\epsilon} \equiv \epsilon / kT$ is the reduced energy.

In Eq. (15) the ensemble average, represented by $<>$, is to be taken over *all* attempts to add the test particle, both those for which there are no hard core overlaps and those for which hard core overlaps do occur. In the latter case $\Delta E^{\mathrm{test}} = \infty$ and the corresponding exponential in Eq. (15) should be set to zero. For example, for $\hat{\epsilon} = 0$, which is the hard sphere limit, the quantity $\langle \exp(\nu \hat{\epsilon}) \rangle$ reduces to the ratio of the number of successful attempts to add a test particle to the total number of attempts.

We now introduce the reduced chemical potential $\hat{\mu}(\phi, T)$, defined as

$$\hat{\mu} \equiv \ln \phi - \ln \langle \exp(\nu \hat{\epsilon}) \rangle. \tag{16}$$

We can see from Eq. (15) that $\mu = kT\hat{\mu} + \mu_0 + E_p^{0,w} - \gamma E_w^{0,w}$. Since the last three terms of this expression will cancel in Eqs. (6) and (7), the phase diagram is determined entirely by $\hat{\mu}$. In fact, we can replace μ with $\hat{\mu}$ in Eqs. (6) and (7). As a shorthand, we will refer to $\hat{\mu}$ as the chemical potential. We use Monte Carlo simulations to calculate the quantity $\langle \exp(\nu \hat{\epsilon}) \rangle$.

(ii) We assume that the chemical potential may be represented by an analytic form, which we use to explicitly carry out the integration in Eq. (7). We will see in the next section that the error introduced by this approach in the reconstruction of the phase diagram is small, whereas the savings in computational time are great. We fit the Monte Carlo results to the following expression for $\hat{\mu}(\phi, T)$:

$$\hat{\mu}(\phi, T) = \hat{\mu}_{\mathrm{CS}}(\phi) + \sum_{n=1}^{n_0} A_n(T) \phi^n. \tag{17}$$

Here,

$$\hat{\mu}_{\mathrm{CS}} = \ln \phi - 3 + \frac{3 - \phi}{(1 - \phi)^3}. \tag{18}$$

In Eq. (18), $\hat{\mu}_{\mathrm{CS}}$ is the Carnahan–Starling[31] approximation for the chemical potential of an assembly of hard spheres. The $A_n(T)$ of Eq. (17) are temperature-dependent coefficients to be determined. The parameter n_0 is chosen so as to obtain a smooth representation of the chemical potential. If n_0 is too large, the fit tends to follow in detail the statistical errors of the Monte Carlo simulation. On the other hand, for small n_0 the systematic deviation of the fit from the Monte Carlo results becomes large. We therefore typically choose $n_0 = 4$. Note that for $\hat{\mu}(\phi, T)$ to have the correct high temperature behavior (i.e., to reduce to the hard sphere

limit), $A_n(T)$ must, to within the accuracy of the Carnahan–Starling approximation [Eq. (18)], tend to zero as $\epsilon/kT \to 0$. The form of the chemical potential, as given in Eq. (17), was chosen not only because it has the correct high temperature limit, but also because it properly reproduces the low ϕ behavior and it conveniently reduces to the mean field theory result if we set $n_0 = 1$.

We estimate T_c by extrapolating the chemical potential, as explained below, downward in temperature until we find a point where both Eqs. (8) and (9) are satisfied. We perform accurate Monte Carlo simulations at a temperature T_1, where T_1 is within one percent above our estimated T_c, to find $\hat{\mu}(\phi, T_1)$. We then use the extrapolation procedure described in the next paragraph to obtain a series of chemical potential isotherms for temperatures below T_c. Using these isotherms we are able to find the locations of the phase boundaries without any further time-consuming simulations.

To perform the temperature extrapolation, we expand the chemical potential at a temperature $T_2 < T_1$ in powers of $\Delta\hat{\epsilon} \equiv \hat{\epsilon}_2 - \hat{\epsilon}_1$ with $\hat{\epsilon}_1 \equiv \epsilon/kT_1$ and $\hat{\epsilon}_2 \equiv \epsilon/kT_2$. Here we take advantage of the fact that the chemical potential is a function of temperature only through the reduced energy $\hat{\epsilon}$. To first order we have

$$\hat{\mu}(\phi, T_2) = \hat{\mu}(\phi, T_1) + \Delta\hat{\epsilon} \left. \frac{\partial \hat{\mu}}{\partial \hat{\epsilon}} \right|_{\hat{\epsilon}_1}. \tag{19}$$

By substituting Eq. (14) into the definition of the chemical potential in Eq. (16), the derivative $\partial\hat{\mu}/\partial\hat{\epsilon}$ may be written as

$$\frac{\partial \hat{\mu}}{\partial \hat{\epsilon}} = \frac{1}{\epsilon} \left(\frac{\partial \bar{E}_{\text{int}}}{\partial N_p} \right)_{V,T}, \tag{20}$$

where $\bar{E}_{\text{int}}$ is the average interaction energy of the system. Using Eq. (3) we have

$$\bar{E}_{\text{int}} = -\bar{N}_{\text{con}}\epsilon = -\tfrac{1}{2} N_p \bar{\eta} \epsilon. \tag{21}$$

Here $\bar{N}_{\text{con}}$ is the average number of protein–protein contacts and $\bar{\eta}$ is the average number of contacts per particle. Substituting Eq. (21) into Eq. (20), we re-express Eq. (19) as

$$\hat{\mu}(\phi, T_2) = \hat{\mu}(\phi, T_1) - \frac{\Delta\hat{\epsilon}}{2} \frac{\partial}{\partial \phi} [\phi \bar{\eta}(\phi, T_1)]. \tag{22}$$

The quantity $\bar{\eta}(\phi, T_1)$ is also calculated during the Monte Carlo simulation at temperature T_1. Note that $\bar{\eta}$ is not equal to $\langle \nu \rangle$, the ensemble average of the number of contacts made by the test particle, for the test particle is not in thermodynamic equilibrium with the other particles in the system.

Therefore, once we have performed the Monte Carlo simulation at temperature T_1, we construct $\hat{\mu}(\phi, T_2)$ by using Eq. (22). We have found empirically that we may reliably employ our temperature expansion provided that $\Delta\hat{\epsilon}/\hat{\epsilon}_1$ is less than ten percent. At each temperature we fit the Monte Carlo results for the chemical potential (both those obtained by direct simulation and those obtained from our extrapolation procedure) by Eq. (17) with the appropriate values of the coefficients $A_n(T)$. Once we have an analytic representation for the chemical potential we use Eqs. (6) and (7) to calculate the coexisting phases at each temperature and hence obtain the coexistence curve. In this way, we have calculated the critical volume fraction ϕ_c, the reduced critical energy $\hat{\epsilon}_c$, the spinodal and the coexistence curve, for a large number of square-well reduced ranges λ between 1.05 and 2.40.

For the Monte Carlo simulation we randomly place our particles inside a cube of unit volume with the usual periodic boundary conditions.[32] The hard core diameter, σ, of the particles was chosen to be in the range 0.14–0.18, so that we have $N = 100$–250 particles at the highest volume fractions $\phi = 0.3$–0.4 for which we perform the simulation. Note that here $\phi \equiv \frac{1}{6}\pi\sigma^3 N$. To generate a statistical ensemble of configurations, the particles are displaced using a time-saving modification of the well-established NVT Metropolis scheme.[33] In our scheme, as in the Metropolis scheme, the displacement of a particle is accepted unconditionally if the change in the total energy of the system, ΔE, due to the displacement, is negative and with probability $\exp(-\Delta E/kT)$ if ΔE is positive. From the ensemble so generated, we may calculate the quantities $\bar{\eta}$ and $\langle \exp(\nu\hat{\epsilon}) \rangle$ which are needed in Eqs. (16) and (22) to obtain chemical potential isotherms. The quantity $\langle \exp(\nu\hat{\epsilon}) \rangle$ is found through the addition of test particles to the system. To accumulate statistically significant information on the average value of $\exp(\nu\hat{\epsilon})$, we must continue testing each configuration of the system until, on average, at least one successful attempt to add a test particle is made. A successful attempt is one for which the core of the test particle does not overlap with that of any other particle. Thus, the addition of test particles not only enables us to calculate the quantity $\langle \exp(\nu\hat{\epsilon}) \rangle$, but also provides information on acceptable new positions for the particles of the system. Using this information, in our scheme we generate new members of the ensemble (as described in the following paragraph) by moving particles to any acceptable position inside the simulation volume. This should be contrasted with the standard choice for particle displacement. Usually, the step size for particle displacement is chosen in such a way that approximately half of the trial configurations are accepted. This is the rule of thumb to optimize the speed of evolution of the system. However, since we are only interested in the chemical potential, we may use the same information for chemical potential tests and particle repositioning. In this way the system evolves several times faster than in the standard (small step size) algorithm. Naturally, the results of the two methods are the same. The use of the same information for chemical potential tests and particle repositioning in no way biases the results; if we refrain from calculating the chemical potential we simply have a Metropolis equilibration algorithm.

The fundamental cycle in our Monte Carlo simulation consists of the following sequence of steps: (i) A particle is selected at random. (ii) An attempt is made to add a new test particle at a randomly chosen position. (iii) If the attempt is successful, the number of contacts made by the test particle is calculated. (iv) For a successful attempt, or an unsuccessful one where the test particle *only* overlaps with the single particle selected in step (i), the next configuration is created by moving the particle chosen in step (i) to the position of

TABLE I. Results and parameters from the Monte Carlo simulations at different reduced ranges λ (λ=∞ is the mean field limit). The quantities presented are (i) the critical volume fraction ϕ_c; (ii) the reduced critical energy $\hat{\epsilon}_c$; (iii) the average number of contacts per particle at the critical point $\bar{\eta}_c$; (iv) the number of successful attempts made $K_{\rm tot}$ in units of 10^6; (v) the reduced energy at which the simulation is performed $\hat{\epsilon}_1$; (vi) the diameter of the particles σ; (vii) the maximum number of particles used in the simulation $M_{\rm max}$; and (vii) the maximum volume fraction $\phi_{\rm max}$.

λ	ϕ_c	$\hat{\epsilon}_c$	$\bar{\eta}_c$	$K_{\rm tot}$	$\hat{\epsilon}_1$	σ	$M_{\rm max}$	$\phi_{\rm max}$
∞	0.134	0.000	∞	0.5	0.000	0.16	178	0.38
∞	0.132	0.000	∞	0.9	0.000	0.14	248	0.36
2.40	0.140	0.197	15.51	1.0	0.195	0.16	140	0.30
2.40	0.140	0.197	15.64	4.7	0.196	0.14	208	0.30
2.20	0.135	0.263	11.81	2.9	0.260	0.14	228	0.33
2.20	0.135	0.262	11.59	1.7	0.260	0.16	140	0.30
2.00	0.126	0.361	8.58	4.1	0.357	0.14	218	0.31
2.00	0.126	0.359	8.45	3.0	0.357	0.16	142	0.30
1.80	0.132	0.487	6.71	6.0	0.480	0.16	148	0.32
1.80	0.129	0.483	6.46	7.7	0.480	0.18	118	0.36
1.65	0.146	0.610	5.95	7.3	0.608	0.16	142	0.30
1.65	0.149	0.606	5.95	9.1	0.605	0.18	110	0.34
1.50	0.171	0.763	5.38	12.8	0.760	0.18	110	0.34
1.50	0.166	0.773	5.33	5.5	0.767	0.16	154	0.33
1.40	0.172	0.935	4.85	3.4	0.930	0.14	218	0.31
1.40	0.173	0.922	4.72	20.6	0.920	0.18	100	0.31
1.30	0.194	1.129	4.44	15.5	1.127	0.18	110	0.34
1.30	0.193	1.128	4.41	6.7	1.127	0.18	110	0.34
1.25	0.205	1.269	4.27	21.5	1.267	0.18	110	0.34
1.25	0.206	1.270	4.31	14.0	1.267	0.18	100	0.31
1.20	0.219	1.449	4.17	5.5	1.435	0.16	169	0.36
1.20	0.216	1.443	4.09	17.1	1.435	0.18	110	0.34
1.15	0.227	1.693	3.91	10.7	1.680	0.16	169	0.36
1.15	0.227	1.673	3.83	24.0	1.660	0.18	110	0.34
1.10	0.235	2.035	3.54	31.9	2.015	0.16	169	0.36
1.10	0.244	2.038	3.63	61.6	2.015	0.18	118	0.36
1.05	0.246	2.667	3.16	122.1	2.650	0.18	125	0.38
1.05	0.273	2.665	3.42	81.4	2.650	0.18	125	0.38

the test particle. This last move is accepted in the standard way, i.e., it is accepted unconditionally if the change in energy due to the move, ΔE, is negative and with probability $\exp(-\Delta E/kT)$ if ΔE is positive.

We see that the test particle of step (ii) can be thought of as simply a label for the position to which we are trying to move the particle chosen in step (i). By steps (i), (ii), and (iv), we generate the members of the canonical ensemble. Furthermore, during step (iii), the test particle is also used to calculate the chemical potential of the system by means of Widom's formula [see Eqs. (11) and (16)]. The algorithm we have outlined above is significantly faster than one in which the evolution of the system, through small steps, is carried out independently of the calculation of the chemical potential.

For a given reduced range λ, we performed our main Monte Carlo simulation at a reduced energy, $\hat{\epsilon}_1 \equiv \epsilon/kT_1$, within one percent below the reduced critical energy, $\hat{\epsilon}_c \equiv \epsilon/kT_c$, as shown in Table I. The critical energy was estimated from auxiliary simulations by using the temperature extrapolation method. Our main simulation was continued until the statistical errors in $\hat{\mu}$ were no greater than the uncertainties associated with the analytic fit of $\hat{\mu}$ [Eq. (17)].

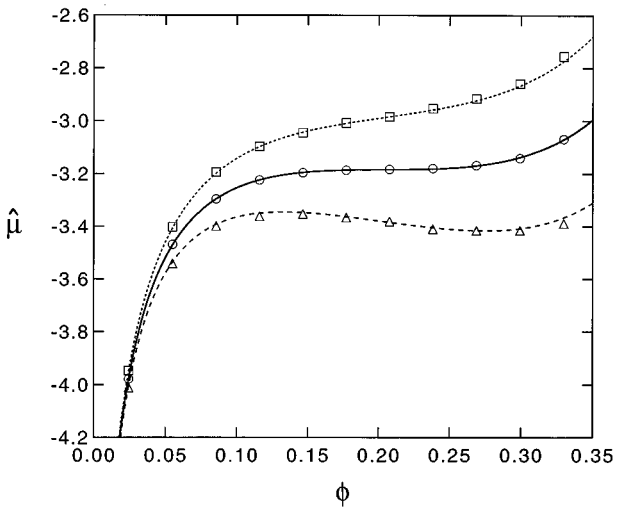

FIG. 1. Illustration of the temperature expansion method for λ=1.25. The open symbols represent the Monte Carlo results for the chemical potential for three different values of the reduced energy $\hat{\epsilon}=1.318$ (triangles), 1.267 (circles), and 1.216 (squares). The solid line is a fit to the $\hat{\epsilon}=1.267$ Monte Carlo results using Eq. (17) with $n_0=4$. The dashed lines are the chemical potentials obtained by extrapolating the $\hat{\epsilon}=1.267$ chemical potential to $\hat{\epsilon}=1.318$ (coarse dashed line) and to $\hat{\epsilon}=1.216$ (fine dashed line).

As usual, the system was allowed to equilibrate before testing for the chemical potential. Extrapolation and fitting techniques were used, as explained previously, to obtain the phase diagram. It should be noted that the final determination of ϕ_c and $\hat{\epsilon}_c$ is made by a small extrapolation of the results from the thorough simulation carried out at $\hat{\epsilon}_1$. Thus, systematic errors in these quantities are very small. The whole procedure was repeated for a large number of reduced ranges $1.05 \leqslant \lambda \leqslant 2.40$.

In the next section we present the results of our Monte Carlo study.

III. RESULTS AND DISCUSSION

A. Results of this study

We begin our discussion by illustrating our temperature extrapolation method. In Fig. 1 we compare the direct Monte Carlo results for the chemical potential with those obtained by extrapolation. The open symbols represent the simulation results of the chemical potential for λ=1.25 at three different values of the reduced energy $\hat{\epsilon}=$ 1.318 (triangles), 1.267 (circles), and 1.216 (squares). The dashed lines are the chemical potentials obtained by extrapolating the chemical potential at $\hat{\epsilon}=1.267$ to $\hat{\epsilon}=1.318$ (coarse dashed line) and to $\hat{\epsilon}=1.216$ (fine dashed line) using Eq. (22). The solid line is the analytic fit of Eq. (17) with $n_0=4$ to the $\hat{\epsilon}=1.267$ Monte Carlo results. We see that the chemical potentials obtained by extrapolating from $\hat{\epsilon}=1.267$ to either $\hat{\epsilon}=1.318$ or $\hat{\epsilon}=1.216$ (i.e., ±4% of the original temperature) are in satisfactory agreement with those calculated directly at $\hat{\epsilon}=1.318$ and $\hat{\epsilon}=1.216$ by Monte Carlo simulation. We find similar agreement between the simulation results and the extrapolation method over the whole range of λ studied, $1.05 \leqslant \lambda \leqslant 2.40$.

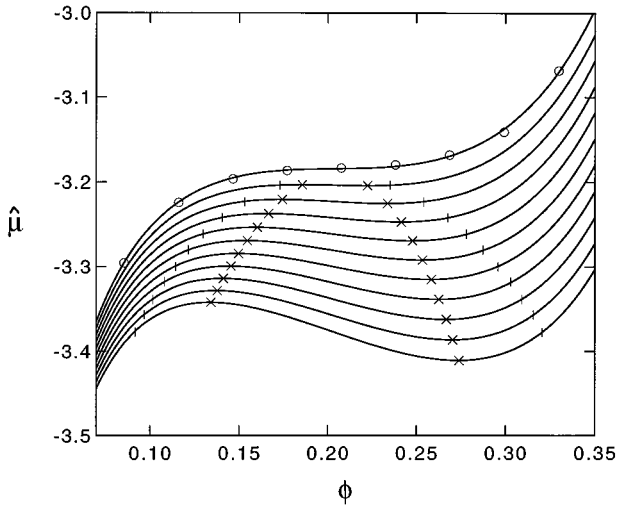

FIG. 2. Reconstruction of the spinodal and the coexistence curve. The open circles are the Monte Carlo results for the chemical potential with $\lambda=1.25$ and $\hat{\epsilon}=1.267$. The isotherms which result from the temperature extrapolation (from $\hat{\epsilon}=1.267$ to $\hat{\epsilon}=1.317$ in steps of 0.005) are shown as solid lines. The coexisting points and spinodal points at each temperature are shown as dashes and crosses, respectively.

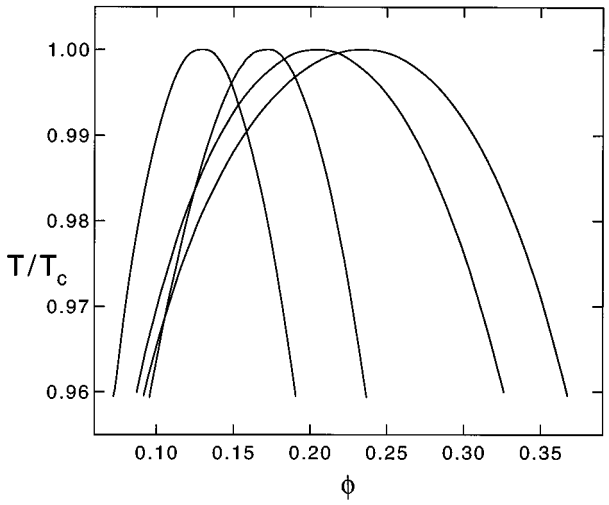

FIG. 3. Coexistence curves. The curves with progressively larger widths represent the results obtained for the reduced ranges $\lambda=1.8$, 1.5, 1.25, and 1.1.

This gives us confidence to use the extrapolation procedure in place of the many time-consuming simulations that would otherwise be required.

The coexisting volume fractions may then be determined from the chemical potential isotherms by applying Eqs. (6) and (7). The points which lie on the spinodal are given by Eq. (10). An example of the construction of the coexistence curve and spinodal is shown in Fig. 2 for the case $\lambda=1.25$. The open circles are the Monte Carlo results for the chemical potential with $\lambda=1.25$ and $\hat{\epsilon}=1.267$. The isotherms which result from the temperature extrapolation (from $\hat{\epsilon}=1.267$ to $\hat{\epsilon}=1.317$ in steps of 0.005) are shown as solid lines. The coexisting points and spinodal points at each temperature are shown as dashes and crosses respectively. The coexistence curves so constructed are shown in Fig. 3 for the reduced ranges $\lambda=1.8, 1.5, 1.25$, and 1.1. The coexistence curves become broader as the range of the interaction decreases, and the corresponding critical volume fraction increases.

In Table I we list the results for a group of representative Monte Carlo simulations for different values of the reduced range, λ. For each value of λ listed in column 1, we present in columns 2–4 the corresponding results we obtained for the critical volume fraction ϕ_c, the critical reduced energy $\hat{\epsilon}_c \equiv \epsilon/kT_c$, and the average number of contacts per particle, $\bar{\eta}_c$, at the critical point. Note that all the results in the table were obtained using $n_0=4$. The manner in which we obtained the results in the $\lambda=\infty$ case will be discussed in Sec. III C.

To gain insight into the accuracy of the results, we varied the conditions under which the simulations were made. We list in columns 5–9 of Table I the simulation parameters that we varied; K_{tot}, the total number of successful attempts (in units of 10^6) made during the testing of the chemical potential at each volume fraction, the reduced energy, $\hat{\epsilon}_1$, at which the simulation is performed, σ, the diameter of the particles, $M_{\max}$, the maximum number of particles used in the simulation, and $\phi_{\max}$, the maximum volume fraction at which the simulation was carried out (note that $\phi_{\max}=M_{\max}\pi\sigma^3/6$). For each reduced range presented in Table I, we show the results obtained with two different sets of simulation parameters. Although it is difficult to evaluate *a priori* the systematic errors inherent in our method, we may estimate *a posteriori* our errors by using the variation in the values of the quantities of interest; the critical volume fraction ϕ_c, the reduced critical energy $\hat{\epsilon}_c$, and the average number of contacts per particle at the critical point $\bar{\eta}_c$. We see that these quantities vary by no more than a few percent between the different runs for a given λ.

Another source of systematic errors which we investigated is that brought about by our particular choice of fit to Eq. (17). Different fits will result in different values for the critical volume fraction and the critical temperature. In Table II we show the values of ϕ_c and $\hat{\epsilon}_c$ obtained using different values of n_0 at three different ranges, $\lambda=1.8$, 1.3, and 1.1. We see that the variation in ϕ_c and $\hat{\epsilon}_c$ due to the change in n_0 is of the order of the errors shown in Table I. Thus we

TABLE II. Variation of the simulation results with the order of the chemical potential fit, n_0.

λ	n_0	ϕ_c	$\hat{\epsilon}_c$
1.80	3	0.126	0.466
1.80	4	0.129	0.483
1.80	5	0.132	0.484
1.30	3	0.189	1.131
1.30	4	0.194	1.129
1.30	5	0.196	1.132
1.10	3	0.251	2.006
1.10	4	0.244	2.038
1.10	5	0.245	2.038

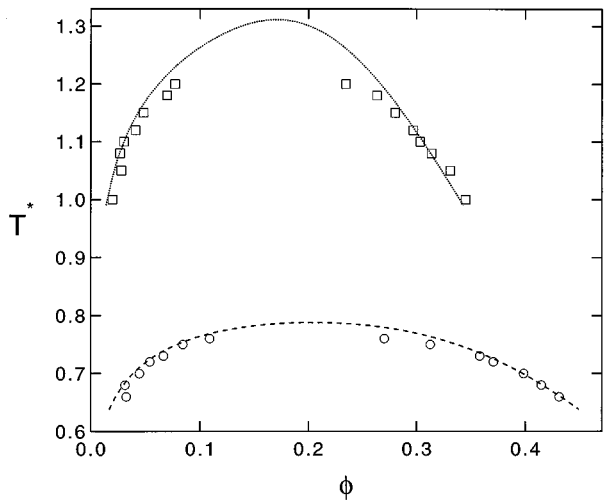

FIG. 4. Comparison of the coexistence curves. The coexistence curves from our simulations at $\lambda=1.25$ (coarse dashed line) and 1.5 (fine dashed line) are shown together with the coexisting points obtained by Vega *et al.* (Ref. 24) for the same ranges (open circles and squares, respectively). Note that $T^*=kT/\epsilon$.

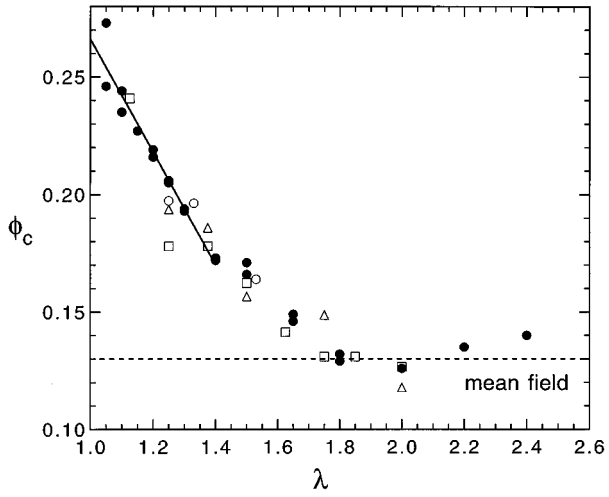

FIG. 5. Variation of the critical volume fraction with the reduced range. Our results (solid circles) are presented together with those of Henderson *et al.* (Ref. 22) (open squares), Vega *et al.* (Ref. 24) (open triangles), and Lomba *et al.* (Ref. 26) (open circles). The solid line is a linear extrapolation of our results to $\lambda=1$. The dashed line is the mean field result.

conclude that, for $n_0=3$, 4, or 5, our results are relatively insensitive to the value of n_0 chosen. However, we do find that for n_0 below three the fit does not give an adequate representation of the chemical potential, while for n_0 above five, the fit begins to follow the statistical errors of the simulation results.

B. Other Monte Carlo results

In view of the nonorthodox nature of our calculational procedure, which involves analytic techniques as well as simulations, it is useful to compare our results with those available from conventional Monte Carlo simulations. We present, in Fig. 4, the coexistence curves from our simulations at $\lambda=1.25$ (coarse dashed line) and 1.5 (fine solid line), together with the coexisting points for the same values of λ as obtained by Vega *et al.* (open circles and squares, respectively).[24] We can see that the agreement between the two simulations is satisfactory, even though we extend our coexistence curves to temperatures significantly below the critical point. Note that $T^*=kT/\epsilon$.

We believe that our approach provides a better way to estimate ϕ_c and $\hat{\epsilon}_c$ than the conventional Monte Carlo method. As can be seen from Fig. 4, the Gibbs ensemble Monte Carlo simulations of two coexisting phases[24] are impractical to carry out close to the critical point. Therefore, the critical parameters of those calculations must still be obtained from some form of extrapolation. Our simulations are carried out very close to the critical temperature allowing for a better estimation of ϕ_c and $\hat{\epsilon}_c$.

In Figs. 5 and 6 we compare our deduced critical volume fractions and reduced critical energies with those found by conventional Monte Carlo simulations. In Fig. 5, we show our results (solid circles) for the critical volume fraction ϕ_c as a function of the reduced range λ. We also show in Fig. 5 the results for ϕ_c, as obtained by other Monte Carlo simulations: (i) Henderson *et al.*[22] use an NVT algorithm (open squares); (ii) Vega *et al.*[24] use a Gibbs ensemble Monte Carlo simulation (open triangles); (iii) Lomba *et al.*[26] use a Gibbs ensemble Monte Carlo simulation but choose a Yukawa potential instead of a square-well (open circles). The corresponding results for the reduced critical energy $\hat{\epsilon}_c$ are shown in Fig. 6. We have converted the Yukawa potential parameters into those of an equivalent square-well by taking the depth of the two potentials to be the same and requiring the high temperature limit of the second virial coefficients to be equal. The Yukawa potential results of Lomba *et al.*[26] illus-

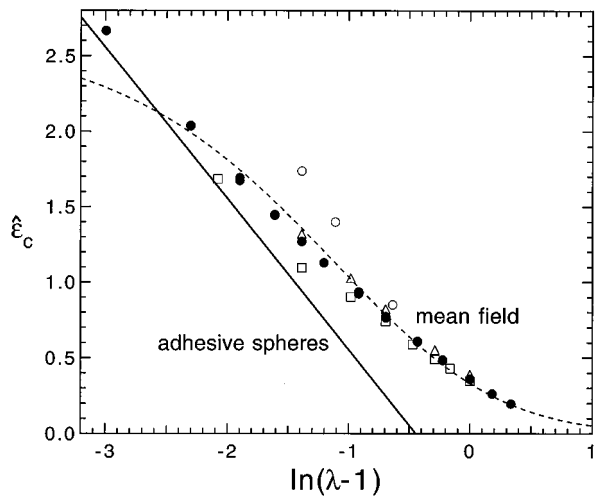

FIG. 6. Variation of the critical reduced energy with the reduced range λ. Our results (solid circles) are presented together with those of Henderson *et al.* (Ref. 22) (open squares), Vega *et al.* (Ref. 24) (open triangles), and Lomba *et al.* (Ref. 26) (open circles). The solid line is Eq. (29) with $\tau_c=0.13$. The dashed line is Eq. (28) with $a_c=10.6$.

trate that the phase separation phenomena do not depend on the detailed form of the potential chosen. We see that the mean values we find for ϕ_c and $\hat{\epsilon}_c$ are consistent with those found by others. In addition, the uncertainty in our results is smaller than that obtained by conventional Monte Carlo simulations.

The effectiveness of our approach is especially important for short range potentials which are the focus of our study. Monte Carlo simulations become increasingly time-consuming as $\lambda \to 1$.[23] However, the time saved by our use of analytic methods allows us to thoroughly investigate the short range regime as can be seen from Fig. 5.

C. Connection with the mean field and adhesive sphere models

As we have seen above, our Monte Carlo calculations provide a description of the phase diagram over a wide domain of λ, $1.05 \leqslant \lambda \leqslant 2.40$. It is interesting to examine these Monte Carlo results in the $\lambda \to \infty$ and $\lambda \to 1$ limits where analytic solutions are available. The $\lambda \to \infty$ limit corresponds to mean field theory,[34] while the $\lambda \to 1$ limit corresponds to the adhesive or sticky sphere model.[15,16] Both of these ''limiting'' theories depend on one parameter only. We will show how the general two parameter ($\hat{\epsilon}$ and λ) square-well potential reduces to these different one parameter models. We show that we can recover the well-known mean field results[8,20] and we determine the domain of λ in which mean field theory becomes a valid approximation. For the $\lambda \to 1$ limit, the Monte Carlo calculation provides us with important estimates of the critical parameters of the adhesive sphere model, which have been the subject of theoretical uncertainty.[16]

The connection between the two parameter square-well potential and the two limiting theories is most readily seen by considering the second virial coefficient $B_2(T)$ of the square-well potential,[35] where

$$B_2 = -\frac{3}{\pi\sigma^3}\int_0^\infty \{\exp[-u(r)/kT]-1\}d^3r$$

$$= -4\{[\exp(\hat{\epsilon})-1](\lambda^3-1)-1\}. \tag{23}$$

For the interaction between the proteins to provide a physically reasonable equation of state, B_2 must be finite. In the mean field case, this requirement implies that as $\lambda \to \infty$, we must have $\hat{\epsilon} \to 0$ [see Eq. (23)]. Analogously, for the adhesive sphere model, we must take $\hat{\epsilon} \to \infty$ as $\lambda \to 1$. Therefore, the second virial coefficients for the two limiting theories are

$$B_2^{\mathrm{mf}} = -4(\hat{\epsilon}\lambda^3 - 1),$$

$$\text{for mean field } (\lambda \to \infty, \hat{\epsilon} \to 0), \tag{24}$$

$$B_2^{\mathrm{ad}} = -4[3(\lambda-1)\exp(\hat{\epsilon})-1],$$

$$\text{for adhesive spheres } (\lambda \to 1, \hat{\epsilon} \to \infty). \tag{25}$$

Equations (24) and (25) provide relationships between $\hat{\epsilon}$ and λ for the two limiting theories. Thus, if we define the quantities

$$a = 4\hat{\epsilon}\lambda^3 \tag{26}$$

and

$$\tau = \frac{1}{12(\lambda-1)\exp(\hat{\epsilon})}, \tag{27}$$

we see that a is the single parameter which characterizes the mean field theory, while τ is the single parameter which describes the adhesive sphere model. Note that a corresponds to the well known van der Waals term[34] and is a measure of the strength of the attraction between particles for a long range interaction potential. The parameter τ, introduced by Baxter,[15] is a measure of the stickiness of the adhesive spheres. The hard sphere case ($\hat{\epsilon} = 0$) can be regained from either limiting theory; $a \to 0$ in mean field theory or $\tau \to \infty$ for the adhesive sphere model.

We begin our analysis by considering the predictions of these limiting theories for the reduced critical energy, $\hat{\epsilon}_c \equiv \epsilon/kT_c$. In Fig. 6 we show our simulation results (solid points) for the reduced critical energy as a function of $\ln(\lambda-1)$. We see that reduced critical energy increases as the range of the potential decreases. The mean field result for $\hat{\epsilon}_c$ is

$$\hat{\epsilon}_c = \frac{a_c}{4\lambda^3}. \tag{28}$$

This last equation is derived from Eq. (26) and a_c is the value of the parameter a at the critical point. The dashed line in Fig. 6 represents Eq. (28) with $a_c = 10.6$, a value determined analytically.[8,20] We see that mean field theory gives a good estimate for $\hat{\epsilon}_c$ for reduced ranges greater than $\lambda \sim 1.10$ [$\ln(\lambda-1) \sim -2.30$].

As λ tends to unity, we may compare our findings with the adhesive sphere results given by Eq. (27). At the critical point $\tau = \tau_c$ and the relation between $\hat{\epsilon}_c$ and λ is

$$\hat{\epsilon}_c = -\ln[12\tau_c(\lambda-1)]. \tag{29}$$

The numerical value of τ_c is not well-established. Watts *et al.*[16] obtained τ_c by using the Percus–Yevick[14] equation to find an analytic solution for the equation of state[15] of adhesive spheres. They undertook a calculation of the equation of state in three distinct ways; through the pressure, compressibility, and energy equations. The pressure equation gives unphysical solutions while the other two equations predict different values for τ_c; 0.098 (from the compressibility equation) and 0.12 (from the energy equation). Neither of these two values is consistent with our results for $\hat{\epsilon}_c$ as λ approaches unity. For our Monte Carlo results to asymptotically approach the theoretical predictions, we require $\tau_c > 0.125$. We observe that this lower bound for τ_c is larger than either of the two previous estimates made by Watts *et al.*[16] The solid line in Fig. 6 shows a comparison of our results with Eq. (29) for $\tau_c = 0.13$.

We may also examine the behavior of the critical volume fraction in the context of the two limiting theories. In Fig. 5 we show the mean field result for ϕ_c as the horizontal dashed

line, $\phi_c = 0.130$.[8,20] We note that for the mean field theory to give an accurate result for ϕ_c, the reduced range λ must exceed 1.65.

To compare the Monte Carlo findings with the adhesive sphere model, we extrapolate our results for the critical volume fraction to $\lambda = 1$. If we perform a linear extrapolation (solid line), we find that $\phi_c(\lambda = 1)$ is 0.266 ± 0.009. The uncertainty reported in this quantity represents only the statistical errors of our data and does not include any systematic errors. The critical volume fractions predicted by Watts *et al.*[16] are $\phi_c = 0.121$ (from the compressibility equation) and $\phi_c = 0.320$ (from the energy equation). The large uncertainty in the theoretical result is due to the increasing flatness of the chemical potential near the critical point as $\lambda \to 1$. This makes the critical volume fraction very sensitive to the approximations made in the Percus–Yevick scheme. We believe that our result, $\phi_c(\lambda = 1) = 0.266 \pm 0.009$, represents a reliable estimate of the critical volume fraction for adhesive spheres. This value of the critical volume fraction may prove useful as a benchmark for further investigations of systems with short range interactions.

Another quantity we may examine to elucidate the connection between the limiting theories and the Monte Carlo results is $\bar{\eta}$, the average number of contacts per particle. We calculate the dependence of $\bar{\eta}$ on volume fraction during the Monte Carlo simulations. This important quantity is the key ingredient in our extrapolation formula [Eq. (22)]. The low ϕ behavior of $\bar{\eta}$ may be examined theoretically. The result is

$$\bar{\eta} = 8(\lambda^3 - 1)\exp(\hat{\epsilon})\phi. \tag{30}$$

Equation (30) is derived using the Boltzmann distribution and assuming that the particles interact independently.[36] The assumption of independent interactions is also a fundamental postulate in mean field theory and it is justified when the number of possible contacts is large, i.e., $\lambda \to \infty$. Thus, Eq. (30) should hold for all ϕ in the mean field limit and where it reduces to $\bar{\eta}_{\mathrm{mf}} = 8\lambda^3\phi$.

It is by using this last result that we calculated the $\lambda = \infty$ entries in Table I. By substituting the expression for $\bar{\eta}_{\mathrm{mf}}$ into Eq. (22), we obtain the temperature extrapolation formula in the mean field limit, namely,

$$\hat{\mu}(\phi, T_2) = \hat{\mu}(\phi, T_1) - 2\Delta a \phi \tag{31}$$

with $\Delta a \equiv a(T_2) - a(T_1)$ and a is given by Eq. (26). It can be shown from Eq. (16) that Eq. (31) is exact, i.e., higher order terms in Δa tend to zero in the mean field limit. Our $\lambda = \infty$ entries were obtained by using Eq. (31) to extrapolate the chemical potential obtained from a hard sphere [$T_1 = \infty$, $a(T_1) = 0$] simulation. The results shown in Table I agree with those found analytically in the mean field limit.[8,20] We also find $a(T_c) = 10.6$ as predicted theoretically.

In Fig. 7, we show the average number of contacts per particle $\bar{\eta}$ (open symbols), as a function of ϕ for several of the entries in Table I, (i) $\lambda = 1.05$ ($\hat{\epsilon}_1 = 2.650$, triangles); (ii) $\lambda = 1.25$ ($\hat{\epsilon}_1 = 1.267$, squares); (iii) $\lambda = 1.65$ ($\hat{\epsilon}_1 = 0.605$, bow ties); and (iv) $\lambda = 2.20$ ($\hat{\epsilon}_1 = 0.260$, circles). Recall that $\hat{\epsilon}_1$ is the reduced energy at which the simulations are performed. The straight lines represent Eq. (30) with $\hat{\epsilon} = \hat{\epsilon}_1$ at each of the ranges listed above. As expected, Eq. (30) fits the Monte Carlo results very well at low ϕ for all values of λ. For a given range λ, the deviation of $\bar{\eta}$ from the direct proportionality to ϕ expressed in Eq. (30) is a measure of the departure from the mean field limit. The solid line in the figure is the analytic result for $\bar{\eta}$ in the adhesive sphere limit[37] with $\tau = 0.13$. At low ϕ, this full expression reduces to $\bar{\eta} = 2\phi/\tau$, a result which can be obtained directly from Eq. (30). As we see, the average number of contacts per particle provides direct physical insight into the protein interactions. We will return to it in the next section.

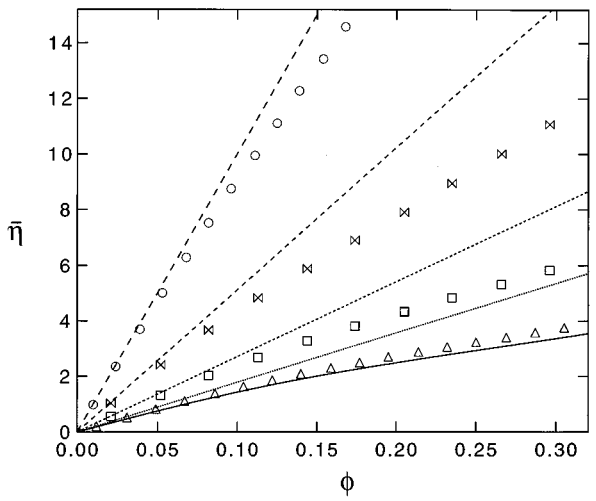

FIG. 7. The average number of contacts per particle. The average number of contacts per particle, $\bar{\eta}$, is shown as a function of ϕ for several ranges, (i) $\lambda = 1.05$, $\hat{\epsilon} = 2.650$ (triangles); (ii) $\lambda = 1.25$, $\hat{\epsilon} = 1.267$ (squares); (iii) $\lambda = 1.65$, $\hat{\epsilon} = 0.605$ (bow ties); (iv) $\lambda = 2.20$, $\hat{\epsilon} = 0.260$ (circles). The straight dashed lines represent the low ϕ behavior for the different ranges as given by Eq. (30). The solid line is the adhesive sphere result for $\tau = 0.13$.

D. Comparison with experimental data for the γ-crystallin proteins

In this section we compare the coexistence curves generated by the Monte Carlo simulation with the experimentally measured ones.[7] In Fig. 8 we present data points of the reduced coexistence curves (T/T_c vs ϕ) for γ_{IIIa} (circles), γ_{IIIb} (squares), γ_{II} (triangles), and γ_{IVa} (bow ties). The experimentally observed value of ϕ_c is 0.21 ± 0.02 for all the γ-crystallins. From Fig. 5, this corresponds to a range of approximately $\lambda = 1.25$. Thus, we also show our Monte Carlo results for the coexistence curves at $\lambda = 1.25$ (coarse dashed line).

For comparison, we also present the mean field coexistence curve as obtained analytically (fine dashed line). Recall that in the mean field case $\phi_c = 0.130$. It is interesting to note that one can understand the experimentally observed value of $\phi_c = 0.21$ as arising from the short range character of the interaction potential. In addition, the Monte Carlo results for $\lambda = 1.25$ predict a coexistence curve which is twice as broad as the one obtained by mean field theory. Nevertheless, the predicted width is still about half that found experimentally.

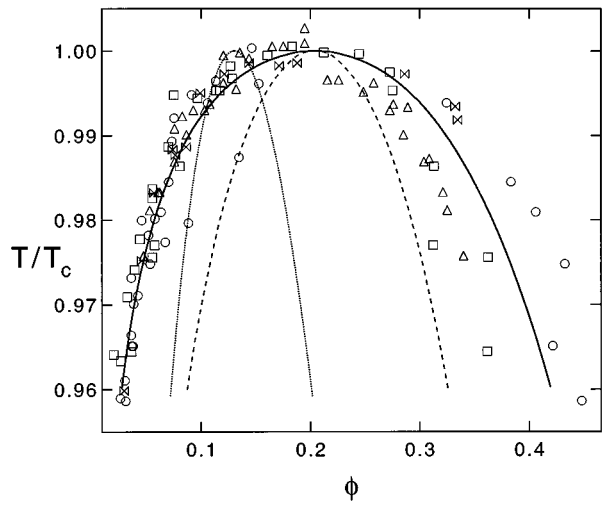

FIG. 8. Comparison with the experimental results for the γ-crystallins. The coexistence curve generated by the Monte Carlo simulation for $\lambda=1.25$ is shown as a coarse dashed line. The fine dashed line represents the coexistence curve obtained analytically in the mean field limit. The experimental results of Broide *et al.* (Ref. 7) are presented for γ_{IIIa} (circles), γ_{IIIb} (squares), γ_{II} (triangles), and γ_{IVa} (bow ties). The solid line is the coexistence curve obtained for $\lambda=1.25$ and a temperature dependent interaction energy of the form $\epsilon=kT_c\hat{\epsilon}_c[1+\kappa(T-T_c)/T_c]$, with $\kappa=-3$.

Even if we allow for uncertainty in the value of the critical volume fraction, and hence consider smaller values of λ, we still find that the curves generated by Monte Carlo simulation are significantly narrower than the experimental coexistence curves.

The question of the ''extra width'' of the coexistence curves notwithstanding, it is important to note that the agreement between the Monte Carlo simulations and the experiment results worsens as λ increases. Therefore, it is safe to conclude that the range of the protein–protein interaction is no greater than $\lambda=1.25$. Since the γ-crystallins are typically 48 Å in diameter, this sets an upper limit of 12 Å on the width of the attractive well of the γ-crystallins. This is consistent with the conclusions drawn from structure factor measurements.[38] The information contained in Figs. 3, 5, and 7 shows that λ must exceed 1.65 for mean field theory to provide a satisfactory description of the protein–protein interactions. Our observation above that $\lambda\leqslant 1.25$ for the γ-crystallins implies that a mean field model is inappropriate for studying γ-crystallin phase separation.

We now examine possible explanations for the width of the experimentally determined coexistence curves. Since the interaction between the proteins is in fact mediated by the surrounding water, we may consider the energy of interaction between the proteins to be temperature dependent. For example, $\epsilon(T)=kT_c\hat{\epsilon}_c[1+\kappa(T-T_c)/T_c]$, where κ is a constant. In Fig. 8, the coexistence curve for $\lambda=1.25$ with $\kappa=-3$ is shown as a solid line. This curve, which obviously gives a better fit to the data than the temperature independent ($\kappa=0$) case, is obtained by appropriately rescaling the $\kappa=0$ coexistence curve. The temperature dependence of the interaction energy in no way affects ϕ_c, but it does increase the width of the coexistence curve. It remains to be seen whether such a strong temperature dependence of $\epsilon(T)$ is physically reasonable.

It is also possible that the observed extra width of the coexistence curve could result from an anisotropic character of the protein interaction energy. We note from our simulations that, as the range of the interaction decreases, $\bar{\eta}_c$, the average number of contacts per particle at the critical point, decreases (see Table I) while the width of the coexistence curves increases (see Fig. 3). Therefore, it is conceivable that for the phase separation curve to become even broader and agree with the experimental observations, the number of contacts should drop below the very short range results. This will occur if the true potential is both short-ranged and anisotropic.

From these considerations an interesting point emerges. We can see from the results presented in Table I that for a system with short range attractions ($\lambda\rightarrow 1$) each particle already makes only about three contacts at the critical point. An anisotropic potential, i.e., one for which the attraction between proteins depends on their relative orientation, will cause the average number of contacts per particle to drop even further and may change the system to the point where phase separation is replaced by reversible aggregation. The experimental results presented in this section lead us to believe that the proteins we study could be in fact close to this boundary. Therefore, it would be interesting to explore the role of anisotropy in the relationship between phase separation and reversible aggregation.

IV. SUMMARY AND CONCLUSIONS

We have studied the binary liquid phase separation of aqueous protein solutions by modeling the protein interactions with a square-well potential. We utilize this potential in a hybrid Monte Carlo method which blends simulations with thermodynamic extrapolation techniques. In this method, we use the results of Monte Carlo simulations along a single isotherm to construct an analytic form of the chemical potential for a series of isotherms above and below the critical temperature. This unorthodox Monte Carlo scheme permits us, by the economy of its design, to reconstruct the phase diagram of systems over a wide domain of the reduced range of attraction λ. In particular, we have thoroughly explored potentials in the short range regime, with ranges as small as $\lambda=1.05$. These potentials are especially important for they apply to many colloidal suspensions, including the γ-crystallin protein solutions which we have previously investigated experimentally.

Our results provide insight into the central role played by the range of the interaction in determining the shape and location of the phase boundaries. Indeed, we have found that as the range decreases, the width of the coexistence curve increases and the critical volume fraction shifts to higher values. As part of our analysis, we have demonstrated how the two parameter square-well model reduces to the one parameter mean field model as $\lambda\rightarrow\infty$ and to the one parameter adhesive sphere model as $\lambda\rightarrow 1$. In the mean field limit, we

recover the analytic result for the critical volume fraction, $\phi_c(\lambda \to \infty) = 0.13$. In fact, we find that the mean field model is a valid approximation provided that $\lambda \geqslant 1.65$. On the other hand, by examining our short range results, we are able to propose a value for the critical volume fraction in the adhesive sphere limit, $\phi_c(\lambda = 1) = 0.266 \pm 0.009$. We have also obtained an estimate for the critical value of the Baxter parameter $\tau_c \approx 0.13$. In view of the uncertainty in previous analytical findings, we believe that our results will be useful benchmarks for future theoretical and experimental studies of the adhesive sphere system.

For the γ-crystallins, we have experimentally observed a critical volume fraction of $\phi_c \approx 0.21$ and very broad coexistence curves. These facts imply that $\lambda \leqslant 1.25$, that is the width of the attractive well of these proteins is no greater than one quarter of their diameter. Thus, we conclude that the interactions between the proteins fall into the short range regime and cannot be described by a mean field theory. Although our simulation results for the critical volume fraction of short range systems are in agreement with the experimentally observed value, the calculated width of the coexistence curve is still significantly smaller than that found experimentally. We have shown that the extra width of the experimental curves may be explained in terms of a temperature dependent depth of the attractive well. However, a more appealing possibility is that this additional width may be due to anisotropy in the interaction potential. Such anisotropic interactions are to be expected in protein solutions. The calculational simplicity of our hybrid Monte Carlo method should facilitate a systematic examination of the effects of such anisotropic interactions.

ACKNOWLEDGMENTS

We thank Professor Mehran Kardar, Dr. Jayanti Pande, and Dr. George Thurston for valuable suggestions and critical comments. This research was supported by the National Eye Institute of the National Institute of Health under Grant No. 5-R37-EY05127.

[1] G.B. Benedek, in *Human Cataract Formation, CIBA Foundation Symposium 106* (Pitman, London, 1984), p. 237.
[2] W.A. Eaton and J. Hofrichter, in *Advances in Protein Chemistry*, edited by J.T. Edsall, F.M. Richards, and D.S. Eisenberg (Academic, San Diego, 1990), Vol. 40, p. 63.
[3] G.G. Glenner, New England Med. **302**, 1283, 1333 (1980).
[4] G.B. Benedek, Appl. Opt. **10**, 459 (1971).
[5] R.J. Siezen, M.R. Fisch, C. Slingsby, and G.B. Benedek, Proc. Natl. Acad. Sci. USA **82**, 1701 (1985).
[6] P. Schurtenberger, R.A. Chamberlin, G.M. Thurston, J.A. Thomson, and G.B. Benedek, Phys. Rev. Lett. **63**, 2064 (1989).
[7] M.L. Broide, C.R. Berland, J. Pande, O.O. Ogun, and G.B. Benedek, Proc. Natl. Acad. Sci. USA **88**, 5660 (1991).
[8] C.R. Berland, G.M. Thurston, M. Kondo, M.L. Broide, J. Pande, O.O. Ogun, and G.B. Benedek, Proc. Natl. Acad. Sci. USA **89**, 1214 (1992).
[9] J. Pande, A. Lomakin, B. Fine, O. Ogun, I. Sokolinski, and G.B. Benedek, Proc. Natl. Acad. Sci. USA **92**, 1067 (1995).
[10] M.H.G.M. Penders and A. Vrij, Adv. Colloid Interface Sci. **36**, 185 (1991).
[11] M.H.G.M. Penders, A. Vrij, and R. Van der Haegen, J. Colloid Interface Sci. **144**, 86 (1991).
[12] C. Liu, A. Lomakin, G.M. Thurston, D. Hayden, A. Pande, J. Pande, O. Ogun, N. Asherie, and G.B. Benedek, J. Phys. Chem. **99**, 454 (1995).
[13] F. Reif, *Fundamentals of Statistical and Thermal Physics* (McGraw-Hill, New York, 1965), Chap. 8, pp. 306–312 and Chap. 10, pp. 422–428.
[14] J.K. Percus and G.J. Yevick, Phys. Rev. **110**, 1 (1958).
[15] R.J. Baxter, J. Chem. Phys. **49**, 2770 (1968).
[16] R.O. Watts, D. Henderson, and R.J. Baxter, Adv. Chem. Phys. **21**, 421 (1971).
[17] Y. Song and E.A. Mason, J. Chem Phys. **91**, 7840 (1989).
[18] J.P. Hansen and I.R. McDonald, *Theory of Simple Liquids*, 2nd ed. (Academic, London, 1990), Chaps. 5 and 6.
[19] F. del Rio and L. Lira, Mol. Phys. **61**, 275 (1987).
[20] V.G. Taratuta, A. Holschbach, G.M. Thurston, D. Blankschtein, and G.B. Benedek, J. Phys. Chem. **94**, 2140 (1990).
[21] A. Rotenberg, J. Chem. Phys. **43**, 1198 (1965).
[22] D. Henderson, O.H. Scalise, and W.R. Smith, J. Chem. Phys. **72**, 2431 (1980).
[23] W.G. Kranendonk and D. Frenkel, Mol. Phys. **64**, 403 (1988).
[24] L. Vega, E. de Miguel, L.F. Rull, G. Jackson, and I.A. McLure, J. Chem. Phys. **96**, 2296 (1992).
[25] M.H.J. Hagen and D. Frankel, J. Chem. Phys. **101**, 4093 (1994).
[26] E. Lomba and Noé G. Almarza, J. Chem. Phys. **100**, 8367 (1994).
[27] A.Z. Panagiotopoulos, Mol. Phys. **61**, 813 (1987).
[28] A.Z. Panagiotopoulos, N. Quirke, M. Stapelton, and D.J. Tildesley, Mol. Phys. **63**, 527 (1988).
[29] E.A. Guggenheim, *Thermodynamics*, 4th ed. (North-Holland, Amsterdam, 1959), Chap. 4, pp. 156–160; J. Clerk-Maxwell, Nature **11**, 357 (1875).
[30] B. Widom, J. Chem. Phys. **39**, 2808 (1963).
[31] N.F. Carnahan and K.E. Starling, J. Chem. Phys. **51**, 635 (1969).
[32] M.P. Allen and D.J. Tildesley, *Computer Simulations of Liquids* (Clarendon, Oxford, 1989), Chap. 1, pp. 24–27.
[33] N.A. Metropolis, A.W. Rosenbluth, M.N. Rosenbluth, A.H. Teller, and E. Teller, J. Chem. Phys. **21**, 1087 (1953).
[34] F. del Rio and L. Lira, J. Chem. Phys. **87**, 7179 (1987).
[35] L.E. Reichl, *A Modern Course in Statistical Physics* (University of Texas, Austin, 1980), Chap. 11, pp. 362–367.
[36] C. Kittel and H. Kroemer, *Thermal Physics*, 2nd ed. (W.H. Freeman and Company, New York, 1980), Chap. 3, pp. 57–63.
[37] Y.C. Chiew and E.D. Glandt, J. Phys. A **16**, 2599 (1983).
[38] B.M. Fine, A. Lomakin, O.O. Ogun, and G.B. Benedek, J. Chem. Phys. (to be published).